Review of Grid-forming Inverters in Support of Power System Operation

Guanhong Song, *Bo Cao and Liuchen Chang*[*]

(Emera and NB Power Research Centre for Smart Grid Technologies, University of New Brunswick, Fredericton E3B 5A3, Canada)

Abstract: The penetration of distributed energy resources in electrical grids has been steadily increasing in an effort to reduce greenhouse gas emissions. Inverters, as interfaces between distributed energy resources and grids, have become critical assets in modern power systems. In recent years, the development and application of grid-forming inverters have gained significant traction due to their capability of supporting power grid operations. A comprehensive review of grid-forming inverters is presented for power system applications. A comparison between grid-forming inverters and grid-following inverters is conducted in terms of their functionalities to highlight the potential of grid-forming inverter technologies in support of power system stability and resiliency. In addition, advanced control strategies integrated into grid-forming inverters under various operation conditions are presented through reviewing the innovations introduced in recent literature and in industrial applications. This paper is intended to provide an updated reference regarding grid-forming inverters for power system applications to researchers and practitioners in the field of power electronics.

Keywords: Grid-forming inverters, grid-forming functions, power conversion

1 Introduction

With increasing public awareness of environmental issues, significant efforts have been made to adopt renewable energy resources for electricity generation to eliminate the use of fossil fuels. Renewable energy-based distributed energy resources (DERs), such as wind [1] and photovoltaics (PV) [2] systems, have been experiencing significant growth in recent decades, and they already play important roles in the electricity market [3-5]. Meanwhile, with the development of energy storage technologies, battery energy storage systems (BESSs) [6] and electric vehicles (EVs) [7] have also become essential power system components contributing to modern power systems. To regulate the operational characteristics of these DERs and perform power conversion that meets the requirements of grid interconnection standards, inverters are the most critical interface required in these systems [8-9].

The high penetration of DERs has brought many system benefits, such as power flow flexibility, ancillary services, and peak shaving, but it also leads to new operation challenges in power grids [10-11]. Conventional DER inverters are generally grid-following (GFL) inverters, which are used to maximize DER power production and feed high quality power to main grids [12-13]. The lack of grid operation considerations in these conventional GFL inverters have brought system stability and reliability issues, as well as control challenges due to their zero-inertia characteristics, lowering the overall inertia of power systems, which makes them vulnerable to grid variations. Although grid-support functions [14-15] and droop control functions [16-18] have been integrated into GFL inverters, which help to shape the power grid under various conditions, they have suffered severe operational limitations because they are only add-ons to GFL inverters and have their control boundaries. Recently, the concept of grid-forming (GFM) has drawn much attention [19-21] because it is primarily developed with enhanced support to power system operations. GFM inverters are generally designed as

Manuscript received July 7, 2021; revised October 2, 2021; accepted November 19, 2021. Date of publication March 31, 2022; date of current version November 29, 2021.
* Corresponding Author, E-mail: LChang@unb.ca
Digital Object Identifier: 10.23919/CJEE.2022.000001

voltage sources that regulate their voltages and frequencies in synergy with power grids through various GFM functions. Droop control functions [22], virtual oscillator control functions [23], and virtual synchronous generator functions [24-25] are the most common functions used in GFM inverters for providing voltage/frequency/inertia support to power grids and for enabling smooth operation with parallel inverters. Other GFM functions have also been developed for GFM inverters, such as the self-synchronization function, coordinated control function, seamless mode transition function, and black-start functions. The self-synchronization function [21] was proposed particularly for two-stage DER-based inverters, integrating DC-link voltage control with droop control functions. The coordinated control function [26] was developed to support the operation of inverters under unbalanced grid conditions. The seamless mode transition function [27] enables flexible operation of a microgrid between grid-connected and islanding operations. Black-start functions [28-29] provide restoration of the power grid from blackout events with practical considerations. With the implementation of these functions, GFM inverters are able to perform grid regulation and thus enhance the grid stability and reliability under various operating conditions.

This paper reviews the functions and state-of-the-art controls of GFM inverters. The remainder of this paper is organized as follows. The differences between these GFM inverters and traditional GFL inverters in terms of control methods under various grid operation scenarios are discussed in Section 2. A review of the primary functions of a GFM inverter is presented and analyzed with recent innovations in GFM technologies in Section 3. Conclusions and recommendations for potential GFM technology advancements are presented in Section 4.

2 Overview of GFM inverter control

Before discussing the built-in functions of GFM inverters, the functional controls are first compared between GFM and GFL inverters [12, 19-30]. Simplified representations of these inverters are presented in Fig. 1, where Fig. 1a shows a grid-connected GFL inverter, Fig. 1b represents a GFM inverter in grid-connected operation, and Fig. 1c depicts a GFM inverter operated in an islanded microgrid. Here, P_{ref}, Q_{ref}, V_{ref}, and f_{ref} are the control references of the active power, reactive power, grid voltage magnitude, and grid frequency, respectively. These control references are usually generated by a system-level controller or a maximum power point tracking (MPPT) algorithm. P^*, Q^*, V^*, and f^* are the modified references generated by the grid-support functions as well as other built-in functions of the inverter. $V(f)$ is the voltage of the grid. $V^*(f^*)$ and $I^*(f)$ are the output voltage and current of the GFM and GFL inverters, respectively. Z_p and Z_s are the equivalent impedances of the GFL and GFM inverters, respectively, and Z_{load} is the sum of all other loads in the network during islanding operation.

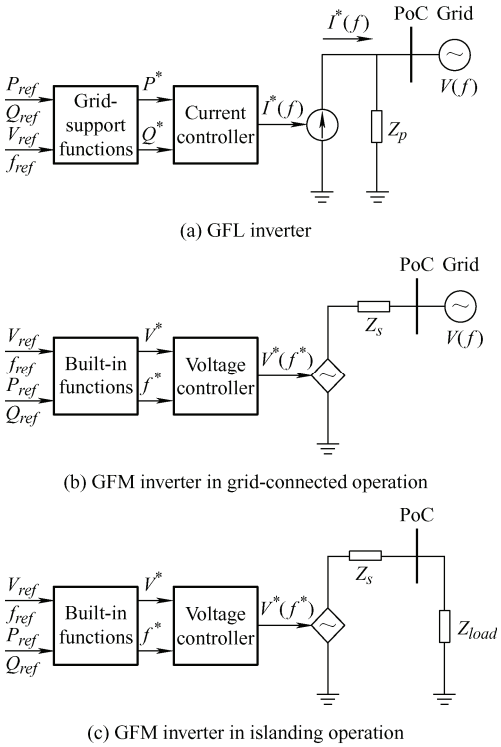

Fig. 1 Simplified representations of GFL and GFM inverters

As shown in Fig. 1a, the GFL inverter can be simplified as an ideal current source connected to the utility grid with parallel high impedance, and it is designed to deliver power from DERs to the grid. Depending on the grid conditions, the control

references of P_{ref}, Q_{ref}, V_{ref}, and f_{ref} from an upper-level controller or an MPPT algorithm are first sent to the grid-support functions, generating the modified power references P^* and Q^*. A current control algorithm is then applied to generate a current command $I^*(f)$ for the inverter operation. Under the GFL operation, only current magnitude and phase angle in the output current are adjusted to achieve the desired active/reactive power outputs. The frequency of the current source remains identical to that of the grid.

Meanwhile, a GFM inverter can be represented as an ideal voltage source and is capable of adjusting the magnitude, frequency, and phase angle of the output voltage in both grid-connected (Fig. 1b) and islanding operation (Fig. 1c).

Similar to a GFL inverter, a GFM inverter may be required to maximize its power production when supplied from a renewable energy source during the normal grid-connected operation. As shown in Fig. 1b, in order to generate the desired output power of the GFM inverter, P_{ref} and Q_{ref} are first sent to the built-in functions, such as a droop controller, leading to the modified references V^* and f^* for the voltage controller to set the output voltage command $V^*(f^*)$ for the GFM inverter. During this operation, the active/reactive power is controlled by adjusting the magnitude, phase angle, and frequency of the GFM inverter output voltage $V^*(f^*)$. Under abnormal grid-connected operations, when the grid voltage or frequency exceeds the limits specified in the grid interconnection standards, the GFM inverter is required to help the power system maintain the desired grid voltage and frequency through direct voltage and frequency regulations. Under these abnormal conditions, grid references V_{ref} and f_{ref} are first sent to the built-in function of the GFM inverter, such as a virtual synchronous generator function [24-25], for the calculation of V^* and f^*. Then, V^* and f^* are further sent to the voltage controller to generate the desired inverter output $V^*(f^*)$ to help the operation of the grid under the abnormal conditions.

Meanwhile, the GFM inverter has significant advantages over the GFL inverter when operated under islanding conditions. The current-source characteristics of a GFL inverter require external voltage sources for its grid synchronization to maintain its normal operation. It suffers from severe operational difficulties in islanding operations without external voltage signals, which cannot be used to solely support or black start an islanding network. On the contrast, a GFM inverter is able to support and black start an islanding network through its capability of providing grid voltage to the islanding network with its voltage-source characteristics [27, 31], as shown in Fig. 1c. Under this islanding condition, the main goal of the GFM inverter is to provide voltage and frequency support to the network by directly controlling $V^*(f^*)$ at their nominal values as a controlled voltage source. The active/reactive power generation from the GFM inverter completely depends on the network load conditions. Moreover, in an islanding network supported by a GFM inverter (usually with weak grid characteristics), other GFM inverters can be easily connected to the network through advanced GFM functions, while GFL inverters may suffer from oscillations when connected to this network due to weak grid variations.

In general, both GFM and GFL inverters have similar grid support and power production goals during grid-connected operation through either active/reactive power adjustments (GFL inverters) or voltage/frequency adjustments (GFM inverters). However, GFM inverters have significant performance advantages over GFL inverters during islanding operations as they not only can be used as voltage sources supporting or black starting the entire islanding network but also have better GFM function integration for the parallel operation in weak islanding grids.

Detailed control block diagrams for both GFL and GFM inverters are shown in Fig. 2. Here, $I(f)$ is the measured grid current, U_{out} is the controller output, and θ is the phase angle of the grid voltage.

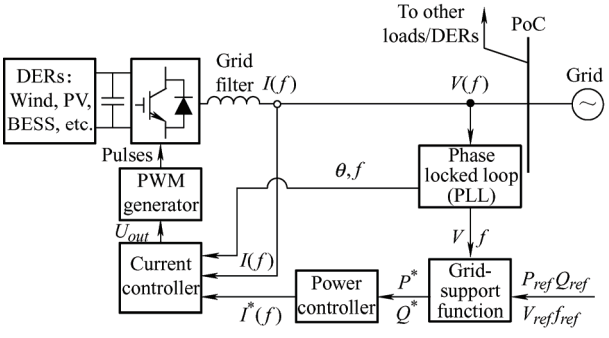

(a) GFL inverter

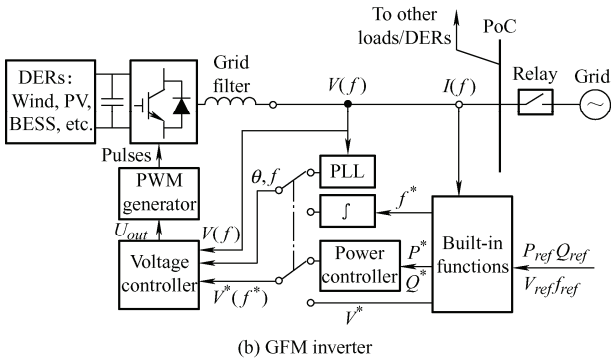

(b) GFM inverter

Fig. 2 Control block diagrams of GFL and GFM inverters

As shown in the block diagram of the GFL inverter in Fig. 2a, grid synchronization is the most critical aspect for smooth power delivery and is usually achieved by phase-locked loop (PLL) algorithms [32-34]. After grid synchronization, control references are sent to each control block to achieve the desired performance.

On the contrary, depending on the control algorithm and operation environment, synchronization is not necessarily required by a GFM inverter, as shown in Fig. 2b. In normal grid-connected operations, the GFM inverter follows the power references from a system-level controller or an MPPT algorithm to generate high-quality power fed to the grid. Meanwhile, when operating under abnormal grid conditions or islanding conditions, the GFM inverter is capable of sustaining its own voltage and frequency based on preset references without the need for a PLL unit. The system references are sent through the built-in function to the voltage controller so that the GFM inverter operates as an active voltage source in supporting the islanding grid operation.

As discussed in this section, GFL inverters are designed mainly to perform power conversion, feeding high-quality power to the grid with grid-support capabilities within the normal grid limits, beyond which the GFL inverters must be disconnected. On the contrary, GFM inverters are not only able to supply power to the utility grid but also have more support functions, such as providing direct voltage, frequency, and inertia support to the utility grid, islanding operation support with seamless mode transitions, for both grid-connected and islanding operations. Detailed descriptions of these GFM functions are provided in Section 3.

3 State-of-the-art GFM functions

To achieve the desired functionality and performance of GFM inverters under different operating conditions, various GFM functions have been developed. In this section, some primary GFM functions integrated in GFM inverters are summarized and explained in detail. In this paper, all the functions are assumed to be built on the control diagram shown in Fig. 2b for GFM inverters.

3.1 Phase-locked loop

The estimation of grid parameters in grid synchronization is necessary in all grid-connected inverters, including both GFL and GFM inverters. Synchronization techniques [32-38] are therefore implemented in these inverters to estimate the grid parameters, such as voltage magnitude, phase angle, and frequency. For a GFM inverter, the accurate estimation of these grid parameters is not only essential for its normal grid-connected operation of delivering power to the grid, but it is also critical to determine suitable GFM functions under abnormal grid conditions and islanding operations.

PLL techniques have been extensively used in grid-connected inverters for synchronizing the output of the inverters with the grid voltage [35-36]. Here, some typical PLL techniques for grid synchronization are reviewed, including synchronous reference frame (SRF) PLL [35-36] and dual second order generalized integrator (DSOGI) SRF-PLL [37] for three-phase GFM inverters, as well as second order generalized integrator (SOGI) SRF-PLL [34, 38] for single-phase GFM inverters.

3.1.1 SRF-PLL

The SRF-PLL method has been widely used in three-phase GFM inverters. The block diagram of an SRF-PLL is presented in Fig. 3, where V_{abc} represents the measured three-phase voltages; v_q is the q-axis voltage extracted from Park's transformation and is sent to a proportional-integral (PI) controller for further processing; ω_{nom}, $\Delta\omega$, and ω are the grid nominal angular frequency, error of the angular frequency and estimated angular frequency, respectively; and θ is the estimated phase angle of the grid voltage. By performing this SRF-PLL, the

frequency, phase angle, and magnitude of the grid voltage can be extracted for inverter output synchronization as well as some other functions and controls. To implement the SRF-PLL into GFM inverters under different grid conditions, improvements were made in Refs. [33, 36-37] for practical implementations.

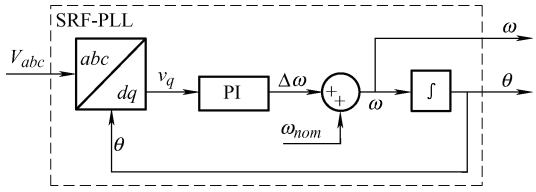

Fig. 3 Block diagram of SRF-PLL

3.1.2 DSOGI-SRF-PLL

Despite the good performance and simple structure of SRF-PLL, it suffers from severe performance degradation under three-phase unbalanced grid conditions [39-40]. A DSOGI-SRF-PLL algorithm was proposed in Ref. [37] to enhance the performance of the original SRF-PLL under unbalanced grid conditions. The block diagram of the DSOGI-SRF-PLL algorithm is presented in Fig. 4, where v_α and v_β are the extracted grid voltages in the $\alpha\beta$ reference frame after Clarke's transformation; K is the damping factor of the SOGI; v'_α, qv'_α, v'_β, and qv'_β are the filtered in-phase and quadrature-phase versions of v_α and v_β, respectively; and $v_\alpha{+}'$ and $v_\beta{+}'$ are the filtered positive sequences of v_α and v_β. Here, the dual SOGI blocks are used to extract and filter in-phase and quadrature-phase voltages of v_α and v_β, while a positive sequence calculator (PSC) is adopted to filter out the unbalance components at these voltages.

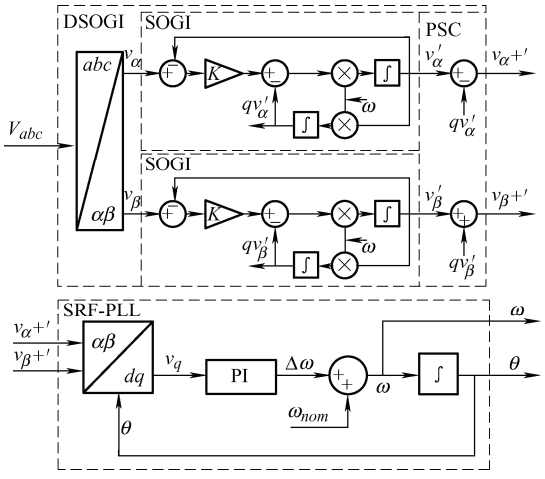

Fig. 4 Block diagram of DSOGI-SRF-PLL

By performing the DSOGI along with PSC, balanced positive sequence voltages in the $\alpha\beta$ frame can be obtained for the SRF-PLL for accurate estimation of the grid magnitude, phase angle, and frequency, even under unbalanced three-phase conditions.

3.1.3 SOGI-SRF-PLL

Single-phase GFM inverters also require grid synchronization during normal grid-connected operations. A PLL algorithm specifically designed for single-phase inverters was proposed in Refs. [34, 38] by adapting the original SRF-PLL algorithm to a single-phase system through an SOGI pretreatment. A block diagram of the SOGI-SRF-PLL algorithm is shown in Fig. 5, where V_α is the measured single-phase grid voltage, and v_α and qv_α are the filtered in-phase and quadrature-phase grid voltages, respectively. By using the SOGI technique, a virtual quadrature-phase voltage is obtained so that the original SRF-PLL can be used to determine the magnitude, phase angle, and frequency of a single-phase voltage.

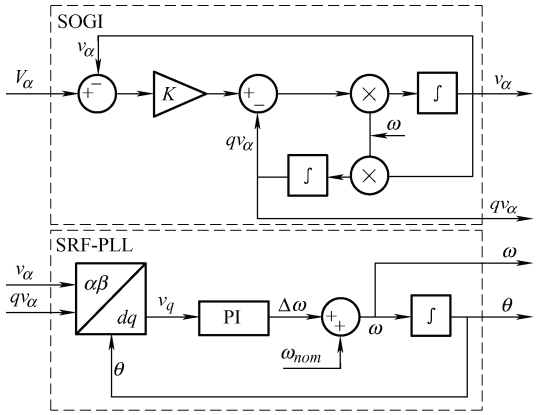

Fig. 5 Block diagram of SOGI-SRF-PLL for single-phase inverters

3.1.4 Other PLL algorithms

Besides the basic PLL algorithms reviewed in Sections 3.1.1-3.1.3, other PLL algorithms have also been proposed and analyzed in the recent Refs. [41-42]. As summarized in Ref. [41], most three-phase PLL algorithms are developed with enhanced filtering capability using loop filter (LF), moving average filter (MAF), notch filter (NF), delayed signal cancelling (DSC) filter, etc., for accuracy improvement of their frequency and phase angle estimations. Meanwhile, the single-phase SOGI orthogonal signal generator-

based (OSG) PLLs have received the most attention recently [42-43], with additional filter design to suppress DC offset and low-order harmonics. Other single-phase PLLs, such as enhanced PLL (EPLL), were also been discussed in Ref. [44] for their detailed performance verification. However, almost all three-phase and single-phase PLLs from recent literature share a common SRF-PLL as their fundamental structure, certain filtering ability, and frequency adaptability.

As discussed in this subsection, PLL algorithms are implemented in inverters to perform grid synchronization through accurate grid frequency and phase angle estimations. Although the basic PLL algorithms, i.e., SRF-PLL, DSOGI-SRF-PLL for three-phase systems, and SOGI-SRF-PLL for single-phase systems, have already been widely used in commercial inverters, they may suffer from performance degradation under practical grid conditions with high DER penetration. Meanwhile, improvements based on these basic PLL algorithms have been made using advanced algorithms to achieve accurate estimation under practical conditions. However, they are usually designed with case-by-case considerations and have suffered heavy computational burden. In general, there exists a trade-off between universality and accuracy in the selection of PLL algorithms for GFM inverters in practical applications.

3.2 Ride-through functions

With the increasing applications of grid-connected inverters in power systems, opportunities have arisen to support the grid operation by these inverters. New standards, such as UL 1741 SA [45], California Rule 21 [46], and IEEE. Std. 1547-2018 [47], were developed and adopted, which included, among other additional requirements, the implementation of fault ride-through functions in all grid-connected inverters [14-15]. A summary of fault ride-through requirements in the recent interconnection standards for grid-connected inverters is presented in Fig. 6, where Fig. 6a outlines the requirements related to grid frequency, and Fig. 6b presents the requirements related to grid voltage. Here, although the GFM inverter uses a voltage controller for grid-connected operation, which acts as a voltage source to the grid, the ride-through functions are still required as guidelines when operating the GFM inverter under different grid conditions. As illustrated in Fig. 6, the operation of the GFM inverter under grid-connected conditions has been divided into several regions with different inverter trip time requirements depending on the grid parameters.

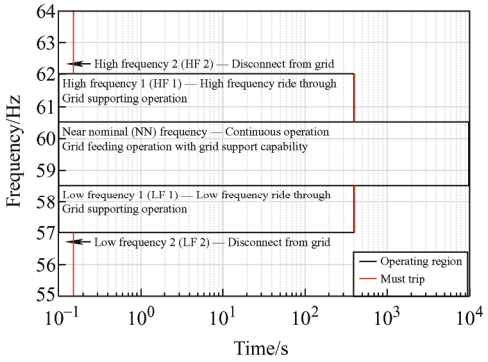

(a) Frequency grid-support and ride-through requirements

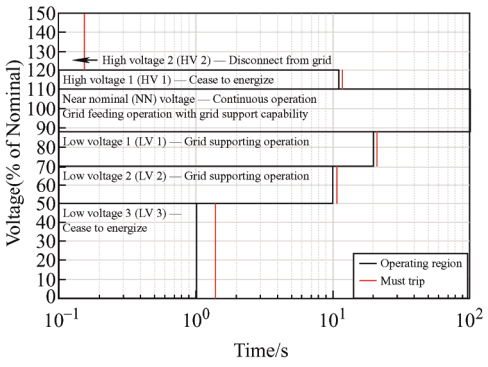

(b) Voltage grid-support and ride-through requirements

Fig. 6 Fault ride-through requirements for grid-connected GFM inverters

In Fig. 6a, the frequency fault ride-through requirements are divided into five regions: near nominal (NN) frequency region, low-frequency 1/2 (LF 1/LF 2) regions, and high-frequency 1/2 (HF 1/HF 2) regions. Similar requirements related to grid voltage fault ride-through can be found in Fig. 6b, where the operations are divided into six regions: NN voltage region, low-voltage 1/2/3 (LV 1/LV 2/LV 3) regions, and high-voltage 1/2 (HV 1/HV 2) regions. Here, GFM inverters have normal operation in the NN region while having abnormal operation in other regions. Each region has its own operational requirements, and different functions can be designed and implemented for each grid condition.

Ride-through functions are therefore required by

GFM inverters to ride-through faults under abnormal grid conditions before disconnecting from the system. As shown in Fig. 6, when GFM inverters operate in the HF 1, LF 1, and LV 1/2 regions, the ride-through functions keep GFM inverters in operation to sustain grid support before disconnecting them from grid until time limits are reached. In these operating regions, GFM inverters are required to directly control their output voltages and frequencies for a relatively long time to help the grid to resume its normal operation. Meanwhile, GFM inverters are also required to cease energizing in a short time (i.e., the must trip time) after the occurrence of a more severe fault, as represented by the HV 1 and LV 3 regions. GFM inverters must also be immediately disconnected from the grid when the grid faults fall into the HF 2, LF 2, and HV 2 regions to prevent severe over-/under-frequency and over-voltage issues.

Under islanding operation for abnormal conditions, ride-through functions are still required by GFM and GFL inverters. Further investigation of the fault ride-through conditions impact of these ride-through actions on the network is required because these islanding microgrids usually have small system inertia and can be easily affected by these ride-through actions.

In general, the ride-through functions are defined by grid interconnection standards with grid-support and protection considerations. However, these ride-through functions originate from a grid-connected GFL inverter, and the implementation of these functions into GFM inverters for both grid-connected and islanding operation requires further modification of grid interconnection standards.

3.3 Droop control

The droop control function of GFM inverters, as was originated from the rotational generators' droop characteristics, has been developed for voltage source operation and supporting grid operations [48-50]. With multiple parallel inverters in operation, the droop control function adjusts the output voltage and frequency of a GFM inverter for synchronizing and power sharing purposes in both grid-connected and islanding operations based on certain droop curves. Here, the operation of the droop control function mainly focuses on adjusting the inverter output in its normal operation, i.e., in the NN region in Fig. 6.

Based on the explanations in Refs. [12, 21, 50], the characteristics of the droop control function are illustrated in Fig. 7, where Fig. 7a is the *P-f* droop curve, and Fig. 7b is the *Q-V* droop curve. Here, V_{nom} and f_{nom} are the grid nominal voltage and frequency, respectively, K_f is the slope (droop rate) of the *P-f* curve, and K_v is the slope (droop rate) of the *Q-V* curve.

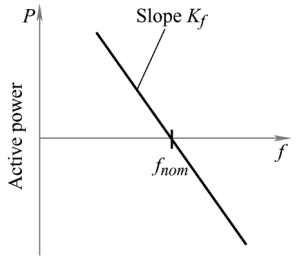

(a) *P-f* curve

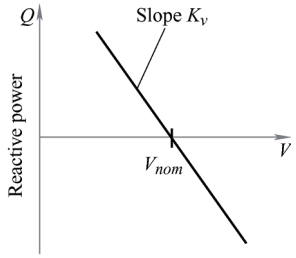

(b) *Q-V* curve

Fig. 7 Droop characteristics

As shown in Fig. 7, the droop equation can be obtained as Eq. (1), where P_{out} and Q_{out} are the output active and reactive power of the GFM inverter, respectively.

$$\begin{cases} f^* = f_{nom} - K_f (P_{out} - P_{ref}) \\ V^* = f_{nom} - K_v (Q_{out} - Q_{ref}) \end{cases} \tag{1}$$

During grid-connected operation with multiple parallel GFM inverters in the network, any disturbances or fluctuations may cause a shift in the operation point resulting in a change in the output power and power sharing between the parallel inverters [21]. The *P-f* droop control function is therefore used to adjust the output frequency of an inverter to prevent the system from further increasing/decreasing its output power, as shown in Fig. 7a. Similar to a rotating synchronous generator (SG), this frequency adjustment alters the phase angle of the inverter voltage, which regulates its active power generation. Meanwhile, the *Q-V* droop control

function is implemented to prevent reactive power circulation within the parallel GFM inverters. By adjusting the magnitude of the inverter output voltage, oscillations in the reactive power generation of the GFM inverter are eliminated, and thus the circulation currents among these inverters can be minimized. In general, the negative feedback control mechanism of the droop control function guarantees smooth operation for multiple parallel inverters in the network.

The droop control function in Fig. 7 and Eq. (1) is still valid under normal islanding operation (i.e., in the NN region) because GFM inverters remain as voltage sources in the network [51-53]. During this islanding operation, the droop control function adjusts the magnitude and frequency of GFM inverter output voltage so that balanced power flow is achieved in the islanded microgrid.

Although various advanced droop control functions were proposed in the recent Ref. [54] for better droop performance, their primary principle of power sharing for multiple GFM inverters remains the same for normal grid-connected and islanding operations. Moreover, as stated in Ref. [16], further research and development on droop control algorithms for grid inertia support is required for practical implementations in modern power systems with high DER penetration.

3.4 Virtual synchronous generator

A virtual synchronous generator (VSG), which emulates a rotating synchronous generator, is a straightforward control approach for a GFM inverter to provide both voltage and inertia support to the grid. Various methods have been proposed, developed, and improved in Refs. [24-25, 55-58]. The fundamentals of the VSG method lie in the swing equation with virtual inertia and damping factor. The mathematical model of the swing equation for the VSG method is given by Eq. (2), with its associated governor formulated as Eq. (3) [25, 57]

$$P_{in}-P_{out}=J\omega_m\frac{\mathrm{d}\omega_m}{\mathrm{d}t}+D^*S_{base}\frac{\omega_m-\omega_g}{\omega_{nom}} \tag{2}$$

where P_{in} is the virtual input power on the generator shaft, P_{out} is the output power of the GFM inverter, J is the virtual system inertia, D^* is the virtual damping factor in p.u., S_{base} is the power rating of the inverter, ω_m is the virtual rotor angular frequency, ω_g is the angular frequency of the measured voltage, and ω_{nom} is the grid nominal angular frequency, which usually has a value of $2\pi50$ or $2\pi60$ rad/s.

$$P_{in}=P_{ref}-k_p^*S_{base}\frac{\omega_m-\omega_{nom}}{\omega_{nom}} \tag{3}$$

where k_p^* is the droop coefficient in p.u.

By letting $k_p=(k_p^*S_{base})/\omega_{nom}$ and $D=(D^*S_{base})/\omega_{nom}$ and combining Eq. (2) with Eq. (3), the *P-f* relation can obtain as

$$P_{ref}-P_{out}=J\omega_m\frac{\mathrm{d}\omega_m}{\mathrm{d}t}+k_p\left(\omega_m-\omega_{nom}\right)+D(\omega_m-\omega_g) \tag{4}$$

Based on Eq. (4), the relationship between the active power of GFM inverters and grid angular frequency, i.e., *P-f* control, is obtained from the virtual system inertia and damping effect.

Here, assuming that the virtual system has characteristics of very low inertia and damping factor, i.e., $J\approx0$ and $D\approx0$, Eq. (4) can be further expressed as Eq. (5), which is identical to the *P-f* droop function in Eq. (1). Here, $f_m=\omega_m/2\pi$ is the frequency of the virtual rotor, and $f_{nom}=\omega_{nom}/2\pi$.

$$f_m=f_{nom}-\frac{1}{2\pi k_p}(P_{out}-P_{ref}) \tag{5}$$

Meanwhile, the relationship between the reactive power and voltage magnitude (*Q-V* control) can also be obtained through the VSG model [21]. The mathematical expression of this *Q-V* control is formulated as

$$V^*=\frac{1}{1+T_vs}(V_{nom}+k_v(Q_{ref}-Q_{out})) \tag{6}$$

where T_v is the time constant of excitation, and k_v is a chosen slope.

When assuming that the excitation response is very fast with $T_v\approx0$, Eq. (6) can be simplified as Eq. (7), which is also identical to the *Q-V* expression in Eq. (1).

$$V^*=V_{nom}-k_v(Q_{out}-Q_{ref}) \tag{7}$$

In general, the VSG method is developed to emulate the operation of a synchronous generator with its rotational inertia and damping factor. By implementing the VSG method in GFM inverters, these inverters are equipped with the capability to perform voltage regulation as well as inertia support in both grid-connected and islanding operations.

Moreover, as shown in Eqs. (4)-(7), it can be concluded that the droop control is a particular case of VSG with zero system inertia, damping factor, and excitation constant.

3.5 Virtual oscillator control

Besides the aforementioned droop control and VSG approaches, which are designed in the phasor representation for voltages of GFM inverters, the virtual oscillator control (VOC) is proposed in the time domain by emulating nonlinear oscillator circuits, which only use output current measurements as the oscillator input for voltage control calculations [22-23, 59-61]. A typical implementation of the VOC method proposed in Ref. [59] using the Van der Pol oscillator for a GFM inverter is shown in Fig. 8, where V_c is the virtual capacitor voltage, i_L is the virtual inductor current; σ, L, and C are the virtual conductance, inductance, and capacitance, respectively; α represents the nonlinear characteristics; K_v and K_i are voltage and current scaling factors, respectively; ε is a constant value with the expression $\varepsilon = \sqrt{L/C}$; and ϕ is a fixed user-defined angle, which is typically selected as 0 or π/2.

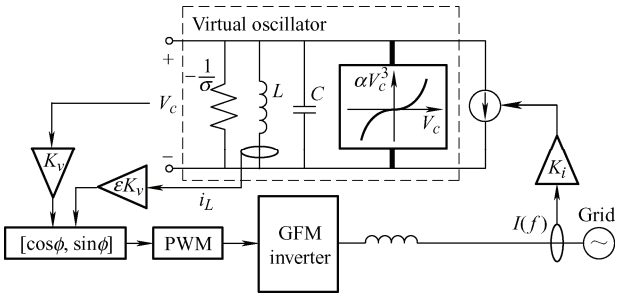

Fig. 8 Typical implementation of virtual oscillator control

The dynamics of the Van der Pol oscillator is expressed as

$$\begin{cases} L\dfrac{\mathrm{d}i_L}{\mathrm{d}t} = V_c \\ C\dfrac{\mathrm{d}V_c}{\mathrm{d}t} = -\alpha V_c^3 + \sigma V_c - i_L - K_i I(f) \end{cases} \tag{8}$$

As shown in Fig. 8 and Eq. (8), only the grid current is measured as the feedback to the VOC, without the need of phasor quantities, such as amplitude, phase angle, and frequency. Based on Ref. [22], the time-domain VOC model can be transformed into a phasor model by averaging the system dynamics over one grid cycle. The averaged dynamics of the VOC method in Ref. [59] is formulated in Eq. (9), where β is a constant defined as $\beta = 3\alpha(K_v^2\sigma)^{-1}$, P and Q are the output active and reactive power of the GFM inverter, respectively.

$$\begin{cases} \dfrac{\mathrm{d}V}{\mathrm{d}t} = \dfrac{\sigma}{2C}\left(V - \dfrac{\beta}{2}V^3\right) - \dfrac{K_i K_v}{2CV}Q \\ \dfrac{\mathrm{d}\theta}{\mathrm{d}t} = \omega = \omega^* - \dfrac{K_i K_v}{2CV^2}P \end{cases} \tag{9}$$

Based on Eq. (9), the relationship between *P-f* and *Q-V* is established for VOC controller design, which regulates the voltage and frequency of the grid through power adjustments of GFM inverters.

In general, the VOC method performs grid voltage regulation based on certain *P-f* and *Q-V* relationships. Different from virtual synchronous generator methods, where the relationship is developed from simulation of a SG, virtual nonlinear oscillators are used by the VOC method to provided such a relationship. However, as stated in Refs. [21, 61], the VOC method has a very fast transient performance, which makes it difficult to perform grid inertia support. Further studies and improvements are required for the implementation of this method in GFM inverters.

3.6 DC-link voltage control

For a typical BESS-based GFM inverter, both the power control and voltage control can be achieved with a single stage [62]. Other DER-based GFM inverters, such as wind and PV inverters, usually require two stages for different control purposes. The DER-side converter regulates the operation of the DERs for maximum power extraction or other control functions, and the grid-side inverter regulates the DC-link voltage as well as the reactive power generation defined by GFM functions [63]. Here, the active power generation from the grid-side inverter is designed to maintain a proper DC-link voltage. A system diagram of a two-stage GFM inverter is presented in Fig. 9, where V_{dc} represents the DC-link voltage.

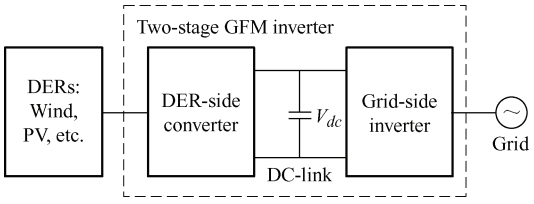

Fig. 9 System diagram of a two-stage GFM inverter

In a two-stage inverter, most VSG and VOC [59-60]

methods cannot be used directly because they require a constant DC source for controlling both the active and reactive power through voltage and frequency adjustments. Although various DC-link control algorithms have been proposed in the recent literature for accurate DC-link voltage control with minimized voltage fluctuations [64-66], these methods are designed mostly for GFL inverters to generate current references and thus require modifications for a GFM inverter. To integrate DC-link control into a two-stage GFM inverter, a self-synchronization technique [21, 67], also known as matching control, has been applied to the synchronous control of GFM inverters, utilizing the dynamics of a DC-link capacitor. To perform DC-link regulation while maintaining its GFM capability, this method [67] integrates a DC-link voltage controller with the frequency droop function in Eq. (1) so that both the DC-link voltage and active power of the two-stage GFM inverter are regulated. A control block diagram of this self-synchronization method [67] is presented in Fig. 10, and the transfer function of this method is formulated in Eq. (10).

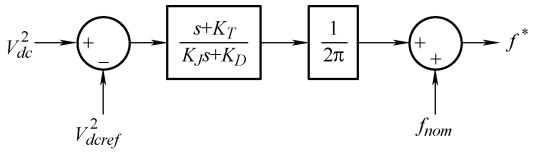

Fig. 10 Block diagram of the self-synchronization method of Ref. [67]

$$f^* = f_{nom} + \frac{s+K_T}{K_J s+K_D}\frac{V_{dc}^2 - V_{dcref}^2}{2\pi} \tag{10}$$

where V_{dcref}^2 is the reference for DC-link voltage, and K_T, K_J, and K_D are coefficients for damping, inertia emulation, and DC-link voltage tracking, respectively.

In general, the self-synchronization function [67] extends the application of droop control from single-stage to two-stage GFM inverters with DC-link regulation consideration. By implementing this function, a relationship between the DC-link voltage and output frequency is established, which synchronizes the regulation of DC-link voltage with the frequency droop control for two-stage GFM inverters. Moreover, future modifications can be made by extending this self-synchronization function with inertia support capabilities for grid performance enhancement.

3.7 Seamless mode transition

The wide applications of inverter-interfaced DERs have brought challenges to power system stability and reliability, due mainly to the reduced system inertia. Microgrids have therefore been introduced into modern power systems as they are capable of performing grid-connected operation as part of the main grid as well as forming an islanded microgrid when disconnected from the main grid. While a microgrid enables flexible and reliable operation of the system under various grid conditions, it also imposes new requirements on GFM inverters. As stated in Ref. [27], to achieve seamless microgrid mode transitions, GFM inverters are required after disconnecting from the grid to support the grid voltage magnitude, grid frequency, network inertia, etc. Meanwhile, they are also required to perform grid synchronization in the process of grid reconnection to minimize inrush voltages and currents during mode changes.

In the recent literature, various mode switching methods [27, 68-74] have been proposed, and they can be divided into two main categories: ① hard-switch mode transition [27, 68-72] and ② cascaded mode transition methods [73-74]. Representative block diagrams of both categories are presented in Fig. 11, where Fig. 11a is a diagram of the hard-switch method, and Fig. 11b is a diagram of the cascaded method.

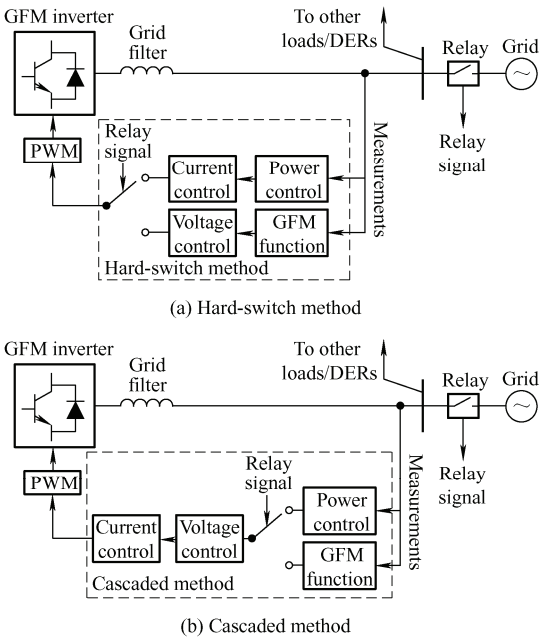

Fig. 11 Block diagrams of seamless transition methods

As shown in Fig. 11a, hard-switch methods have two separate controllers selected by a simple control switch for mode transitions. During grid-connected operation, a GFL-based current controller is used for power delivery following certain power commands, and a voltage controller with GFM functions is used in the inverter for its islanding operation, regulating the network as a voltage source. Mode transition is achieved by a single mode switch, which synchronizes with the grid breaker. Although hard-switch methods have proven their simplicity and effectiveness, there exist severe inrush voltages and currents due to the initialization issues of control variables during mode transitions.

Cascaded methods have been proposed in Refs. [73-74]. This method has a common cascaded grid voltage and current controllers shared by both operation modes. The mode transition in this method is achieved by switching between power control for grid-connected operation and GFM functions for islanding operation. From the controller perspective, this mode change can be seen as voltage reference step changes, and thus the initialization issues during mode changes are eliminated.

In general, seamless mode transition forms a bridge linking the grid-connected operation and islanding operation of the GFM inverter following detailed operational requirements. With such a mechanism, smooth mode changes are achieved with a minimized impact on the entire system.

3.8 Black-start function

With the high penetration of DERs and development of GFM techniques, the potential of GFM inverters for providing black-start support to grids has surfaced [28-29]. The black-start function is a process in the grid restoration strategy to restore a grid from power outages without any support from external grids [75]. Considering the fact that GFM inverters are capable of providing support as virtual synchronous generators, the implementation of the black-start function in GFM inverters has recently drawn the attention of researchers, particularly for microgrid applications [76-78]. Although different black-start configurations have been proposed [29], the most practical GFM-based black-start configurations are ① a fully functional black start using a single BESS-based GFM inverter for the initial black-start procedure and ② a collective black start, where multiple DER-based GFM inverters collectively black start a microgrid. The detailed configurations of these GFM-based black-start strategies are shown in Fig. 12, where the fully functional black-start configuration is shown in Fig. 12a, and the collective black-start configuration is presented in Fig. 12b.

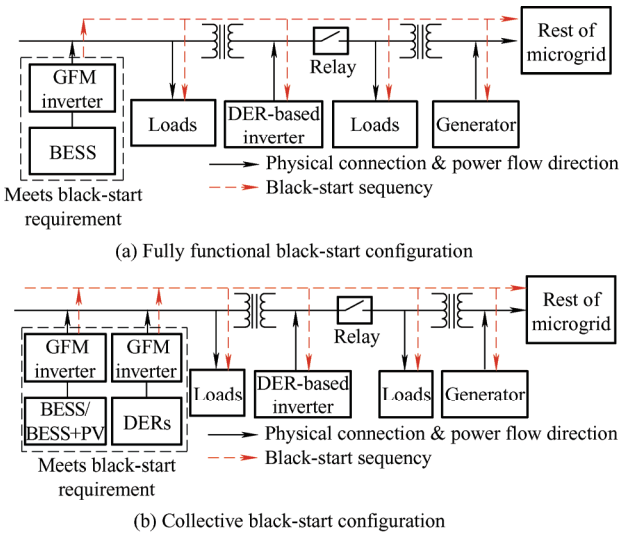

Fig. 12 Detailed configurations of black-start strategies

As illustrated in Fig. 12, the initial black-start procedure is performed by either a single GFM inverter (Fig. 11a) or by stacking multiple smaller GFM inverters (Fig. 11b), which meets all black-start requirements specified by the system operator to support the grid with initial voltage, frequency, inertia, etc. The collective black-start configuration has improved inverter redundancy with low system cost by stacking multiple smaller GFM inverters compared to the fully functional configuration with a single inverter. However, load-sharing and synchronization among these parallel GFM inverters, which are enabled through droop control, VSG, etc., have become the main focuses for practical realization. After the build-up of initial voltage provided by these DER- or BESS-based GFM inverters, other loads, DER-based inverters, and generators can be reconnected to the microgrid following certain restoration strategies, resuming the normal operation of the microgrid from a blackout event.

In general, the black-start function provides GFM inverters with initial voltage built-up capabilities to

support grid restoration from power outages. However, as noted in Ref. [27], the start sequence and synchronization of GFM inverters in this initial procedure of the collective black-start configuration remain as future work, requiring a more detailed investigation for practical applications.

4 Conclusions

With increasing DER penetration, GFM inverters are increasingly required to operate in a GFM mode in exploring the potentials for supporting power system operation and improving reliability and resiliency. This paper presented an overview of the characteristics of GFM inverters by comparison with those of traditional grid-following inverters, and the recent innovations in GFM inverter technologies were highlighted, summarizing the benefits and opportunities of GFM inverters for grid interactive operations under different scenarios.

Significantly more research and development efforts are still required to build on and expand the applications of GFM inverters in support of grid operation of modern power systems dominated by inverter-interfaced DERs. More promising technologies are necessary for GFM inverters to contribute materially to large interconnected systems (i.e., continental-scale power systems). By incorporating a variety of GFM inverters into large electric grids, the overall system dynamics, stability, and failure modes of the system could be affected; therefore, more research on advanced GFM functions with interconnection techniques (e.g., coordinated control function, and black start function) is required for these GFM inverters. In addition, more pilot projects of GFM inverter applications are also required to validate the capabilities of GFM inverters, taking into account the grid contingency and end-to-end system performance.

References

[1] R Vijayapriya, P Raja, M P Selvan. A modified active power control scheme for enhanced operation of PMSG-based WGs. *IEEE Trans. Sustain. Energy*, 2018, 9(2): 630-638.

[2] A Jäger-Waldau. PV Status Report 2019, EUR 29938 EN, Publications Office of the European Union, Luxembourg, 2019, ISBN 978-92-76-12608-9, doi: 10.2760/326629, JRC118058.

[3] REN21. Renewables 2020 Global Status Report (Paris: REN21 Secretariat), 2020, ISBN 978-3-948393-00-7.

[4] IRENA (2018). Renewable capacity statistics 2018, International Renewable Energy Agency (IRENA), Abu Dhabi.

[5] REN21. 2017 Renewables Global Futures Report: Great debates towards 100% renewable energy (Paris: REN21 Secretariat), ISBN 978-3-9818107-4-5.

[6] IRENA (2015). Battery Storage for Renewables: Market Status and Technology Outlook, International Renewable Energy Agency (IRENA), Ruud Kempener.

[7] IEA (2021). Global EV Outlook 2021, IEA, Paris https://www.iea.org/reports/global-ev-outlook-2021.

[8] Q Liu, T Caldognetto, S Buso. Review and comparison of grid-tied inverter controllers in microgrids. *IEEE Trans. Power Electro.*, 2020, 35(7): 7624-7639.

[9] G Wang, G Konstantinou, C D Townsend, et al. A review of power electronics for grid connection of utility-scale battery energy storage systems. *IEEE Trans. Sustain. Energy*, 2016, 7(4): 1778-1790.

[10] M S Alam, F S Al-Ismail, A Salem, et al. High-level penetration of renewable energy sources into grid utility: Challenges and solutions. *IEEE Access*, 2020, 8: 190277-190299.

[11] B Mohandes, M S El Moursi, N Hatziargyriou, et al. A review of power system flexibility with high penetration of renewables. *IEEE Trans. Power Syst.*, 2019, 34(4): 3140-3155.

[12] J Rocabert, A Luna, F Blaabjerg, et al. Control of power converters in AC microgrids. *IEEE Trans. Power Electron.*, 2012, 27(11): 4734-4749.

[13] W Du, F Tuffner, K P Schneider, et al. Modeling of grid-forming and grid-following inverters for dynamic simulation of large-scale distribution systems. *IEEE Trans. Power Deliv.*, 2020, 36(4): 2035-2045.

[14] S Xu, Y Xue, L Chang. Review of power system support functions for inverter-based distributed energy resources-standards, control algorithms, and trends. *IEEE Open J. Power Electron.*, 2021, 2: 88-105.

[15] X Zhao, L Chang, R Shao, et al. Power system support functions provided by smart inverters: A review. *CPSS Trans. Power Electron. Appl.*, 2018, 3(1): 25-35.

[16] X Meng, J Liu, Z Liu. A generalized droop control for grid-supporting inverter based on comparison between traditional droop control and virtual synchronous generator control. *IEEE Trans. Power Electron.*, 2019, 34(6): 5416-5438.

[17] Q C Zhong, G C Konstantopoulos. Current-limiting droop control of grid-connected inverters. *IEEE Trans. Ind. Electron.*, 2017, 64(7): 5963-5973.

[18] M S Golsorkhi, D D C Lu. A control method for inverter-based islanded microgrids based on V-I droop characteristics. *IEEE Trans. Power Deliv.*, 2015, 30(3): 1196-1204.

[19] R H Lasseter, Z Chen, D Pattabiraman. Grid-forming inverters: A critical asset for the power grid. *IEEE J. Emerg. Sel. Top. Power Electron.*, 2020, 8(2): 925-935.

[20] B Mirafzal, A Adib. On grid-interactive smart inverters: Features and advancements. *IEEE Access*, 2020, 8: 160526-160536.

[21] P Unruh, M Nuschke, P Strau, et al. Overview on grid-forming inverter control methods. *Energies*, 2020, 13(10): 2589-2609.

[22] B Johnson, M Rodriguez, M Sinha, et al. Comparison of virtual oscillator and droop control. *2017 IEEE 18th Workshop on Control and Modeling for Power Electronics (COMPEL 2017)*, Stanford, CA, USA, Aug. 2017: 1-1.

[23] M A Awal, H Yu, S Lukic, et al. Droop and oscillator based grid-forming converter controls: A comparative performance analysis. *Front. Energy Res.*, 2020, 8: 168-183.

[24] J Xiao, Y Jia, B Jia, et al. An inertial droop control based on comparisons between virtual synchronous generator and droop control in inverter-based distributed generators. *Energy Reports*, 2020, 6: 104-112.

[25] H Xu, C Yu, C Liu, et al. An improved virtual inertia algorithm of virtual synchronous generator. *J. Mod. Power Syst. Clean Energy*, 2020, 8(2): 377-386.

[26] Y Peng, Y Li, K Y Lee, et al. Coordinated control strategy of PMSG and cascaded H-bridge STATCOM in dispersed wind farm for suppressing unbalanced grid voltage. *IEEE Trans. Sustain. Energy*, 2021, 12(1): 349-359.

[27] M Ganjian-Aboukheili, M Shahabi, Q Shafiee, et al. Seamless transition of microgrids operation from grid-connected to islanded mode. *IEEE Trans. Smart Grid*, 2020, 11(3): 2106-2114.

[28] J Marchgraber, W Gawlik. Investigation of black-starting and islanding capabilities of a battery energy storage system supplying a microgrid consisting of wind turbines, impedance- and motor-loads. *Energies*, 2020, 13(19): 5170-5193.

[29] H Jain, G S Seo, E Lockhart, et al. Blackstart of power grids with inverter-based resources. *IEEE Power and Energy Society General Meeting (PESGM)*, Montreal, QC, Canada, Aug. 2020: 1-1.

[30] P Roos. A comparison of grid-forming and grid-following control of VSCs. Uppsala: Uppsala University, 2020.

[31] X Huang, K Wang, J Qiu, et al. Decentralized control of multi-parallel grid-forming DGs in islanded microgrids for enhanced transient performance. *IEEE Access*, 2019, 7: 17958-17968.

[32] F Wu, L Zhang, J Duan. A new two-phase stationary-frame-based enhanced PLL for three-phase grid synchronization. *IEEE Trans. Circuits Syst. II Express Briefs*, 2015, 62(3): 251-255.

[33] B Liu, F Zhuo, Y Zhu, et al. A three-phase PLL algorithm based on signal reforming under distorted grid conditions. *IEEE Trans. Power Electron.*, 2015, 30(9): 5272-5283.

[34] F Xiao, L Dong, L Li, et al. A frequency-fixed SOGI-based PLL for single-phase grid-connected converters. *IEEE Trans. Power Electron.*, 2017, 32(3): 1713-1719.

[35] D Venkatramanan, V John. Dynamic phasor modeling and stability analysis of SRF-PLL-based grid-tie inverter under islanded conditions. *IEEE Trans. Ind. Appl.*, 2020, 56(2): 1953-1965.

[36] L Hadjidemetriou, E Kyriakides, F Blaabjerg. A new hybrid PLL for interconnecting renewable energy systems to the grid. *IEEE Trans. Ind. Appl.*, 2013, 49(6): 2709-2719.

[37] A Ranjan, S Kewat, B Singh. DSOGI-PLL with in-loop filter based solar grid interfaced system for alleviating power quality problems. *IEEE Trans. Ind. Appl.*, 2021, 57(1): 730-740.

[38] M Xie, H Wen, C Zhu, et al. DC offset rejection improvement in single-phase SOGI-PLL algorithms: Methods review and experimental evaluation. *IEEE Access*, 2017, 5: 12810-12819.

[39] L Feola, R Langella, A Testa. On the effects of unbalances, harmonics and interharmonics on PLL systems. *IEEE Trans. Instrum. Meas.*, 2013, 62(9): 2399-2409.

[40] U K Singh, A Basak. Performance study of different PLL schemes under unbalanced grid voltage. *2019 IEEE Region 10 Symposium (TENSYMP)*, Kolkata, India, Jun. 2019: 66-71.

[41] S Golestan, J M Guerrero, J C Vasquez. Three-phase PLLs: A review of recent advances. *IEEE Trans. Power Electron.*, 2017, 32(3): 1894-1907.

[42] S Golestan, J M Guerrero, J C Vasquez. Single-phase PLLs: A review of recent advances. *IEEE Trans. Power Electron.*, 2017, 32(12): 9013-9030.

[43] Y Han, M Luo, X Zhao, et al. Comparative performance evaluation of orthogonal-signal-generators-based single-phase PLL algorithms: A survey. *IEEE Trans. Power Electron.*, 2016, 31(5): 3932-3944.

[44] J Xu, H Qian, Y Hu, et al. Overview of SOGI-based single-phase phase-locked loops for grid synchronization under complex grid conditions. *IEEE Access*, 2021, 9: 39275-39291.

[45] Underwrit. Lab., UL 1741 Supplement SA: Grid Support Utility Interactive Inverters and Converters, 2016.

[46] California Public Utilities Commission, Recommendations for Updating the Technical Requirements for Inverters in Distributed Energy Resources, Smart Invert. Work. Gr. Recomm., 2014.

[47] IEEE 1547-2018: IEEE Standard for Interconnection and Interoperability of Distributed Energy Resources with Associated Electric Power Systems Interfaces, IEEE Std. 1547, 2018.

[48] Y Deng, Y Tao, G Chen, et al. Enhanced power flow control for grid-connected droop-controlled inverters with improved stability. *IEEE Trans. Ind. Electron.*, 2017, 64(7): 5919-5929.

[49] Z Li, C Zang, P Zeng, et al. Fully distributed hierarchical control of parallel grid-supporting inverters in islanded AC microgrids. *IEEE Trans. Ind. Informatics*, 2018, 14(2): 679-690.

[50] K De Brabandere, B Bolsens, J Van den Keybus, et al. A voltage and frequency droop control method for parallel inverters. *IEEE Trans. Power Electron.*, 2007, 22(4): 1107-1115.

[51] Z Shi, J Li, H I Nurdin, et al. Comparison of virtual oscillator and droop controlled islanded three-phase microgrids. *IEEE Trans. Energy Convers.*, 2019, 34(4): 1769-1780.

[52] H Mahmood, D Michaelson, J Jiang. Reactive power sharing in islanded microgrids using adaptive voltage droop control. *IEEE Trans. Smart Grid*, 2015, 6(6): 3052-3060.

[53] H Bevrani, S Shokoohi. An intelligent droop control for simultaneous voltage and frequency regulation in islanded microgrids. *IEEE Trans. Smart Grid*, 2013, 4(3): 1505-1513.

[54] U B Tayab, M A Bin Roslan, L J Hwai, et al. A review of droop control techniques for microgrid. *Renew. Sustain. Energy Rev.*, 2017, 76: 717-727.

[55] J Alipoor, Y Miura, T Ise. Power system stabilization using virtual synchronous generator with alternating moment of inertia. *IEEE J. Emerg. Sel. Top. Power Electron.*, 2015, 3(2): 451-458.

[56] K Shi, H Ye, W Song, et al. Virtual inertia control strategy in microgrid based on virtual synchronous generator technology. *IEEE Access*, 2018, 6: 27949-27957.

[57] J Liu, Y Miura, T Ise. Comparison of dynamic characteristics between virtual synchronous generator and droop control in inverter-based distributed generators. *IEEE Trans. Power Electro.,* 2016, 31(5): 3600-3611.

[58] Y Du, J M Guerrero, L Chang, et al. Modelling, analysis, and design of a frequency-droop-based virtual synchronous generator for microgrid applications. *2013 IEEE ECCE Asia Downunder*, Melbourne, VIC, Australia, Jun. 2013: 643-649.

[59] B B Johnson, M Sinha, N G Ainsworth, et al. Synthesizing virtual oscillators to control islanded inverters. *IEEE Trans. Power Electron.*, 2016, 31(8): 6002-6015.

[60] M Lu, S Dutta, V Purba, et al. A pre-synchronization strategy for grid-forming virtual oscillator controlled inverters. *2020 IEEE Energy Conversion Congress and Exposition (ECCE),* Detroit, MI, USA, Oct. 2020: 4308-4313.

[61] J Li, J E Fletcher, D G Holmes, et al. Developing a machine equivalent inertial response for a virtual oscillator controlled inverter in a machine-inverter based microgrid. *2020 IEEE Energy Conversion Congress and Exposition (ECCE),* Detroit, MI, USA, Oct. 2020: 4314-4321.

[62] M Liu, W Li, C Wang, et al. Reliability evaluation of large scale battery energy storage systems. *IEEE Trans. Smart Grid*, 2017, 8(6): 2733-2743.

[63] S A Amamra, K Meghriche, A Cherifi, et al. Multilevel inverter topology for renewable energy grid integration. *IEEE Trans. Ind. Electron.*, 2017, 64(11): 8855-8866.

[64] L Yin, Z Zhao, T Lu, et al. An improved DC-link voltage fast control scheme for a PWM rectifier-inverter system. *IEEE Trans. Ind. Appl*., 2014, 50(1): 462-473.

[65] J Lu, S Golestan, M Savaghebi, et al. An enhanced state observer for DC-link voltage control of three-phase AC/DC converters. *IEEE Trans. Power Electron.*, 2018, 33(2): 936-942.

[66] M Merai, M W Naouar, I Slama-Belkhodja. An improved DC-link voltage control strategy for grid connected converters. *IEEE Trans. Power Electron.*, 2018, 33(4): 3575-3582.

[67] L Huang, H Xin, Z Wang, et al. A virtual synchronous control for voltage-source converters utilizing dynamics of DC-link capacitor to realize self-synchronization. *IEEE J. Emerg. Sel. Top. Power Electron*., 2017, 5(4): 1565-1577.

[68] C L Chen, Y Wang, J S Lai, et al. Design of parallel inverters for smooth mode transfer microgrid applications. *IEEE Trans. Power Electron.*, 2010, 25(1): 6-15.

[69] G G Talapur, H M Suryawanshi, L Xu, et al. A reliable

microgrid with seamless transition between grid connected and islanded mode for residential community with enhanced power quality. *IEEE Trans. Ind. Appl.*, 2018, 54(5): 5246-5255.

[70] W Zhang, H Liu, W Wang, et al. Seamless transfer scheme for parallel PV inverter system. *IET Power Electron*., 2020, 13(5): 1051-1058.

[71] S Sajadxan, R Ahmad. Model predictive control of dual-mode operations Z-source inverter: Islanded and grid-connected. *2017 IEEE Energy Conversion Congress and Exposition (ECCE),* Cincinnati, OH, USA, Oct. 2017: 4971-4977.

[72] X Li, H Zhang, M B Shadmand, et al. Model predictive control of a voltage-source inverter with seamless transition between islanded and grid-connected operations. *IEEE Trans. Ind. Electron*., 2017, 64(10): 7906-7918.

[73] J Wang, A Pratt, M Baggu. Integrated synchronization control of grid-forming inverters for smooth microgrid transition. *2019 IEEE Power & Energy Society General Meeting (PESGM),* Atlanta, GA, USA, Aug. 2019: 1-5.

[74] J Wang, N C P Chang, X Feng, et al. Design of a generalized control algorithm for parallel inverters for smooth microgrid transition operation. *IEEE Trans. Ind. Electron.*, 2015, 62(8): 4900-4914.

[75] W Sun, C C Liu, L Zhang. Optimal generator start-up strategy for bulk power system restoration. *IEEE Trans. Power Syst.*, 2011, 26(3): 1357-1366.

[76] Y Tang, J Dai, Q Wang, et al. Frequency control strategy for black starts via PMSG-based wind power generation. *Energies*, 2017, 10(3): 358-371.

[77] M Lu, G S Seo, M Sinha, et al. Adaptation of commercial current-controlled inverters for operation with virtual oscillator control. *2019 IEEE Applied Power Electronics Conference and Exposition (APEC)*, Anaheim, CA, USA, Mar. 2019: 3427-3432.

[78] M Braun, J Brombach, C Hachmann, et al. The future of power system restoration: Using distributed energy resources as a force to get back online. *IEEE Power & Energy Mag.*, 2018, 16(6): 30-41.

Guanhong Song (S'19-M'20) received the B.Sc. degree in Electrical Engineering from Southwest Jiaotong University, Chengdu, China, in 2013. And the Ph.D. degree from the University of New Brunswick, Fredericton, NB, Canada, In 2020. He is currently a Postdoctoral Fellow with the Emera and NB Power Research Centre for Smart Grid Technologies at the University of New Brunswick. His current research interests include power electronics, power converters and distributed generation system.

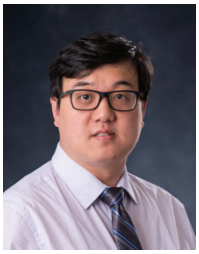

Bo Cao received the B.Sc. degree from East China University of Science and Technology, Shanghai, China, in 2005; and the Ph.D. degree from the University of New Brunswick, Fredericton, NB, Canada, in 2015. He is currently a Research Associate with the Emera and NB Power Research Centre for Smart Grid Technologies at the University of New Brunswick. His principal research interests include power converter design, grid-integration technology, distributed generation system and smart grid techniques.

Liuchen Chang (M'92-SM'99) received B.Sc. degree from Northern Jiaotong University in 1982, M.Sc. from China Academy of Railway Sciences in 1984, and Ph.D. from Queen's University in 1991. He joined the University of New Brunswick in 1992 and is a Professor Emeritus now at UNB. He is a long-time volunteer for IEEE of over 28 years and is the President of the IEEE Power Electronics Society (2021-2022). He is a Fellow of Canadian Academy of Engineering (FCAE). He has published more than 400 refereed papers in journals and conference proceedings. Specializing in power electronics, Dr. Chang has focused on research, development, demonstration and deployment of renewable energy based distributed energy systems and direct load control systems.